Comments on Inorganic Chemistry
Publication details, including instructions for authors and subscription information:
http://www.informaworld.com/smpp/title~content=t713455155

The Prediction of *d-d* Spectra

Malcolm Gerloch[a]
[a] University Chemical Laboratories, Lensfield Road, Cambridge, United Kingdom

To cite this Article Gerloch, Malcolm(1996) 'The Prediction of *d-d* Spectra', Comments on Inorganic Chemistry, 18: 2, 101 — 124
To link to this Article: DOI: 10.1080/02603599608032716
URL: http://dx.doi.org/10.1080/02603599608032716

The Prediction of *d-d* Spectra

MALCOLM GERLOCH
University Chemical Laboratories,
Lensfield Road,
Cambridge CB2 1EW,
United Kingdom

Received July 25, 1995

It is now possible to compute the complete spectral trace for '*d-d*' transitions. Plans for exploiting this within a new teaching and research facility are illustrated. The models upon which the calculations rest are described for the non-specialist researcher.

Key Words: *ligand-field spectra, cellular ligand-field theory, angular overlap model, parity mixing, vibronic coupling, computer simulation*

Abbreviations: *AOM—angular overlap model, CLF—cellular ligand-field, esr—electron spin resonance, LCAO—linear combination of atomic orbitals, NCA—normal coordinate analysis, RMS—root mean square, en—ethylenediamine*

INTRODUCTION

This article describes what I hope will develop into a useful new teaching and research tool deriving from many years of detailed study in ligand-field analysis. It is presented more as "work in progress" than as a finished item. Opportunities for its natural development are discussed at the end.

Comments Inorg. Chem
1996, Vol. 18, No. 2, pp. 101–124
Reprints available directly from the publisher
Photocopying permitted by license only

It concerns the prediction of ligand-field spectra, not just of transition energies but of the complete '*d-d*' spectral trace, together with the computation of the perceived color of a complex. The student might derive help from it for topics like:

- What do the spectra and colors of octahedral and tetrahedral complexes look like for various transition metal ions complexed with various ligand sets?
- How different are these for complexes with less common geometries like the square plane, the trigonal bipyramid or square-based pyramid, and so on?
- What are the spectral consequences of distortions from "ideal" geometries? How do these depend upon the symmetries of such distortions?

Alternatively, a research worker in bioinorganic chemistry, for example, may wish to address questions like:

- Having synthesized or extracted a compound containing a known transition metal center but being unable to grow crystals for X-ray diffraction analysis, the researcher has accumulated evidence which suggests that the coordination is one of three kinds, say. A '*d-d*' spectrum is available. Which of these coordinations is compatible with the spectrum?
- Can evidence from a measurement of circular dichroism help resolve the problem?

We have now produced software which, after only a few seconds of computing time on a Workstation or PC, will provide a full-color graphical answer to such questions. The colored plates at the end of this article show some examples of it (see Color Plates I and II).

The broad features of a typical '*d-d*' spectrum are the position of the bands (the transition energies), the relative intensities of those bands, and their relative bandwidths. All three features must be computed if we are to simulate an experimental spectral trace from a spectrometer. In the next three sections, I provide brief, "broad-brush" accounts for the non-specialist of the models upon which such computations are based. Those already well versed in these matters or, equally, those with little taste for them may prefer to skip straight to the last section in which I detail the use and results of the facility as presently set up.

TRANSITION ENERGIES

The computation of spectral transition energies has occupied researchers in the ligand-field area for many years and is understood both theoretically and practically in considerable detail. An undergraduate course on transition metal chemistry and ligand-field phenomena includes $t_{2g} - e_g$ orbital splitting in O_h symmetry, the combined effects of the ligand field and interelectron repulsion, correlation and Tanabe–Sugano diagrams, as well as various associated magnetic phenomena. Many early studies are of symmetry—and, probably, group theory—not only for historical reasons but also because of the opportunities so provided for exercise in symmetry and structure. More advanced students may learn something also of orbital splitting patterns for planar and bipyramidal geometries but probably not of the many-electron states that accompany them.

Once we enquire about the *d* electron properties of low-symmetry molecules, point group symmetry rapidly loses its usefulness. And, of course, by far the majority of real molecules actually possess little or no symmetry, perhaps because of chemically or spatially inequivalent ligations or because of "unusual" geometries or coordination numbers. Within the ligand-field domain, the most useful model available for the analysis of low-symmetry species is the Angular Overlap Model,[1–4] since reformulated on a sounder theoretical footing as Cellular Ligand-Field theory.[5–10] We should note that no other models currently approach the accuracy of ligand-field theory for the computation of *d*-electron properties.

Ligand-field theory involves nothing more than the manipulation of integrals of molecular states perturbed by operators which act only upon orbitals of *d* character. The operators (components of the energy operator or Hamiltonian) and their integrals are of just three types, referring to *d-d* interelectron repulsions, the ligand-field potential and spin-orbit coupling. Both operators and the wavefunctions upon which they act have radial and angular qualities; for example, *p* and *d* orbitals differ with respect to their angular properties ($l = 1$ or 2, respectively) while 3*d* and 4*d* orbitals differ by virtue of their radial forms. The calculation of the radial parts of both wavefunctions and operators in transition metal complexes is a formidable task which as yet cannot be accomplished with sufficient accuracy for the prediction of spectral properties. Ligand-field computations involve manipulation only of the angular parts of the energy integrals, sequestering all radial parts into parameters. Justifications for so apparently naive a procedure have been given.[7–10]

Interelectron repulsion (ier) and spin-orbit coupling (soc) effects are parameterized on a global level; that is, they refer to the complex molecule as a whole but without recognition of its point-group symmetry. Accordingly, the parameters for ier, F_2 and F_4 (or the Racah equivalents, B and C), and ζ for soc are like their counterparts for the corresponding free metal ions except in magnitude. Departures from the free ion values are measures of charge redistribution on complexation of the metal ion.

By contrast, the ligand-field potential and its associated parameters do carry the molecular geometry and symmetry. The AOM and CLF approaches exploit this in a way that treats all geometries, coordination numbers and molecular symmetries on an equal footing. The central characteristic of these schemes is the spatial superposition of separate contributions to the global (molecular) ligand field that may be reasonably well recognized as chemically discrete. Thus we model each metal-ligand interaction separately and sum their effects throughout the molecule. The summation process takes into account the relative orientations of the various ligations in the complex by transformations that are completely specified by the angular geometry in the whole molecule. All radial information, including bond lengths, therefore resides in *locally* defined parameters.

Consider any one ligation. Conventionally we define a local z axis to be oriented from the metal to the donor atom; x and y axes are chosen along obvious local *pseudo*symmetry axes where appropriate. A typical local reference frame is illustrated in Fig. 1 for a metal-quinoline ligation. Metal d_{z2}, d_{xz} and d_{yz} orbitals referred to this local frame are also shown. As discussed elsewhere,[6] the sources of ligand-field potentials are locally situated, bonding (and antibonding) orbitals which are predominantly of non-d character. A local σ bond perturbs the d_{z2} ($\equiv d_\sigma$) orbital and it suffers an energy shift labelled (parameterized) as e_σ (e for energy, lower case because it refers to an orbital, and σ describing the local *pseudo*symmetry). A local πx bond orbital or ligand function perturbs the d_{xz} ($\equiv d_{\pi x}$) orbital and it suffers an energy shift $e_{\pi x}$. In the local yz plane, we define $e_{\pi y}$ analogously. All δ-type interactions are deemed negligible. The signs of these parameters are determined by the relative energies of the appropriate metal and bonding orbitals and are such that e_λ ($\lambda = \sigma, \pi_x, \pi_y$) are positive for ligands acting as λ donors and negative for λ acceptors. A full, technical account[6] of the origins and physicochemical significance of these and other parameters has been given very recently. By way of example: e_σ(Cl) for a typical Co^{II}-Cl ligation is ca.

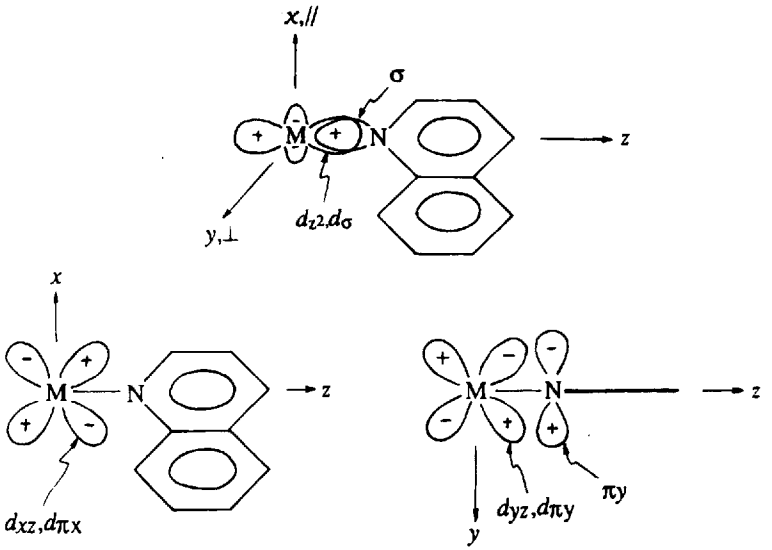

FIGURE 1 Axes and orbitals are defined to reflect features of local electron density.

3000 to 4000 cm^{-1}, but for the more basic amine ligation, Co^{II}-N, is perhaps 4000 to 5000 cm^{-1}. For π interactions, e_π(Cl) in such complexes may be ca. + 800 cm^{-1} and that for e_π (PR_3) is typically –1500 cm^{-1}, so revealing the π acidity of the phosphine ligator. In these examples of so-called "linear ligators", the π interactions are cylindrically symmetric about the M-L bond so that $e_{\pi x} = e_{\pi y} \equiv e_\pi$. For ammonia and amine ligands, it is found that e_π is zero, in agreement with the expected lack of any ligand π function in these species. For Co-quinoline, $e_{\pi\perp}$ (perpendicular to the quinoline ligand plane) is ca. + 500 cm^{-1} while $e_{\pi\parallel} \approx 0$, again in agreement with the absence of any N $p\pi$ orbital *in* the plane of the quinoline moiety. All these parameter values and hundreds like them have been obtained by optimizing calculated molecular properties (spectral transition energies, paramagnetic susceptibilities, esr g values) to corresponding experimental quantities.

Let us return to the question of the summation of local d orbital shifts over all ligands in the complete molecule. Each individual ligation in the complex is parameterized as just described. There is, of course, no question of having N sets of metal d orbitals for N ligations! A unique d orbital set is defined with respect to an arbitrary, but fixed, global (molecular) frame. Then the global d_{z^2} orbital, say, referred to the axis frame

of ligation number 1 looks like a combination of all the locally defined d orbitals: for example, $d_{z2G} \rightarrow 0.4d_{z2L} + 0.1d_{xz}{}^{L} + 0.02d_{yz}{}^{L} + 0.8d_{x^2-y^2}{}^{L} + 0.39\, d_{xy}{}^{L}$. Such coefficients are determined entirely by the relative orientations of the global(G) and local(L) frames and by the angular properties of the d orbitals (defined by $l = 2$). In the present example, the global d_{z^2} orbital therefore suffers an energy shift of $(0.4)^2 e_\sigma(1) + (0.1)^2 e_{\pi x}(1) + (0.02)^2 e_{\pi y}(1)$ (the squares appear because the d functions appear in both bra and ket of the energy integral). The same sort of transformations are carried out for each ligation with the result that each global d orbital suffers a shift that is a combination of e_σ, $e_{\pi x}$ and $e_{\pi y}$, values for each ligation. For the technically minded, we note that off-diagonal matrix elements of the type $\langle d_i | V_{LF} | d_j \rangle$, where i, j mean any member of the d set, must also be related to the local energy parameters in this way and the final global transition energies which are to be compared with experiment are then obtained by diagonalization. For those not so inclined, we note that all observable ligand-field properties—of the whole molecule, of course—are eventually calculated in terms of the complete set of locally defined e_λ parameters, together with the globally defined parameters of interelectron repulsion and spin-orbit coupling.

Research in this area has been analytical. That is to say, the focus has been on the determination of values for all these system variables by optimization of calculated spectral transition energies (and often of paramagnetic properties, too) to those observed. The goal has not so much been the reproduction of experiment as the discovery of underlying features of the bonding in complexes that the various parameter values probe. However, during the course of those many analyses, considerable experience of the signs and magnitudes of CLF parameters has accrued. It is upon this that the completion of the present spectral-prediction facility will be partly based.

INTENSITY DISTRIBUTIONS

Within mainstream inorganic chemistry, ligand-field analysis has barely exploited the information contained in spectral intensities. Two exceptions come to mind, however: the application of polarization selection rules to single-crystal measurements is frequently used to aid assignment, and discrimination between spin-allowed and spin-forbidden transitions is usually possible by virtue of their very different intensities. Detailed,

quantitative analysis of the relative intensities of *d-d* bands, on the other hand, has been largely missing. It is true, of course, that in other chemical disciplines, and within the physics literature, many important contributions[11–21] to this subject have been made. Often these have tackled the problem of *absolute* intensities, however, which is a most difficult task depending, as it does, upon prior calculation of reasonably accurate molecular wavefunctions in transition metal complexes. There is an echo here of the calculation of Δ_{oct} *ab initio*. Ligand-field models elide these difficulties by concentrating solely upon the angular factors involved.

Over the past decade or so, we have constructed an intensity model having the spirit of ligand-field theory as applied to transition energies and which avoids any requirement for radial wavefunctions. Accordingly, we address *relative* intensities or intensity distributions. A central feature of our approach[22] is that of a spatial superposition involving locally defined transition parameters, t_λ, somewhat akin to the locally specified energy parameters, e_λ, of the CLF model. Implicit throughout our approach, by the way, is exclusive attention to electric-dipole transitions in recognition of the very minor role played by magnetic-dipole transitions in ligand-field spectra.

Crucial to the efficacy of the ligand-field approach at large is the markedly small extent of coupling between the *d* orbitals in transition metal complexes (with metals in other than the lowest oxidation states) and all others.[23,24] One important consequence of this is that '*d-d*' transitions involve the rearrangement of *d* electrons against a somewhat constant "background" of all other electrons. To the extent that this is not so—and as indicated by the quotation marks around '*d-d*'—the *d* orbitals lose their purity a little and acquire admixtures of odd-parity functions that relieve the parity selection rule. The weakness of '*d-d*' transitions relative, say, to those which characterize dyestuffs implies that such parity mixing within the '*d*' orbitals is only small. The following discussion develops this point and serves to illuminate the nature of the parity mixing upon which our intensity model focusses.

We consider a molecular orbital, ψ, for a metal *d*–ligand ϕ interaction in the usual LCAO form; for example, for a σ function:

$$\psi_\sigma = c_M d_\sigma + c_L \phi_\sigma. \qquad (1)$$

It is usual to refer the metal orbital (here *d*) to the metal center and the ligand orbital (*s*, *p*, or some combination of these, say) to the ligand center. For present purposes it is more instructive to express all functions

with respect to just one origin—here, the metal atom. The expansion theorem allows one to express any function as an (infinite) sum of convenient basis functions. In the present case, we write the function centered on the ligand as a linear combination of functions centered on the metal:

$$\phi_\sigma^L = a_1 s^M + a_2 p_\sigma^M + a_3 d_\sigma^M + a_4 f_\sigma^M + \cdots. \tag{2}$$

Sharma,[25] for example, has provided explicit expressions for the expansion coefficients in terms of the distance between the centers (the bond length) and of the radial forms of the various basis functions. While we do not require these expressions here, and they form no part of the structure of our parametric model, they do provide a basis for parameter analysis. Figure 2 illustrates how a linear combination of metal-centered orbitals like (2) is able to simulate an orbital on the ligand center. Combining (1) and (2), we arrive at an expression for the $(Md\text{-}L)_\sigma$ orbital referred wholly to the metal center,

$$\psi_\sigma = c_M d_\sigma + b_1 s + b_2 p_\sigma + b_3 f_\sigma + \cdots, \tag{3}$$

and observe that this function possesses the *character* of *s,p,f,* and other orbitals mixed with the *d*. Non-*d* character can also be mixed into the

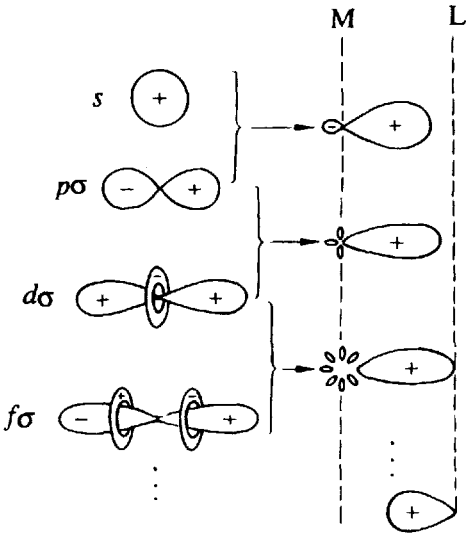

FIGURE 2 Linear combinations of metal σ orbitals progressively reproduce a ligand-centered σ orbital.

parent d function by other means. These might involve functions originating on the metal atom. An expression like (3) will still be appropriate but will fail to discriminate the origins of the non-d character. The intensity model we describe similarly makes no recognition of the origins of d orbital impurity.

The orbital selection rule for electric-dipole transitions identifies allowed intensity as arising between functions related by $\Delta l = \pm 1$. Therefore, we are concerned here only with the odd-parity admixtures into the d orbitals of p and f character. Note, in passing, that our teaching about the violation of the parity selection rule tends only to mention d-p mixing, probably because we focus upon metal d–metal p mixing which is assuredly much larger than metal d–metal f. However, direct metal d–metal p mixing is known[26] to be of far too small a magnitude to account for 'd-d' intensities so that we can usually be confident that the necessary parity mixing arises mostly through the metal-ligand interaction. Accordingly, d-f character mixing is necessarily included in our intensity model on an equal footing with d-p. Once again, the fact that 'd-d' transitions are weak means that *whatever* the origins of the parity mixing, its magnitude is small. This provides one piece of experimental evidence supporting the assertion that coupling between the metal d electrons and others is small. The weakness of 'd-d' transitions is of a piece with the whole ligand-field edifice.[23,24]

Parameterization of the electric-dipole transition moments is straightforward,[22] at least in principle. We consider the electron density displacements suffered during a 'd-d' transition to be expressible as a superposition of local displacements—so echoing the CLF energy scheme. Within a local ligation, we consider an electic-dipole transition between orbitals 'd' and 'd''':

$$\begin{aligned}
\langle \text{`}d\text{'}|\mathbf{er}|\text{`}d''\text{'}\rangle &\equiv \langle d + p + f|\mathbf{er}|d' + p' + f'\rangle \\
&= \langle d|\mathbf{er}|d'\rangle && \text{I} \\
&+ \langle d|\mathbf{er}|p'\rangle + \langle p'|\mathbf{er}|d\rangle && \text{II} \\
&+ \langle d|\mathbf{er}|f'\rangle + \langle f'|\mathbf{er}|d\rangle && \text{III} \\
&+ \langle p + f|\mathbf{er}|p' + f'\rangle && \text{IV} \qquad (4)
\end{aligned}$$

For reasons of simplicity here, we have sequestered the parity mixing coefficients into the functions labelled d, p and f. Now integrals I vanish identically because of the orbital and parity selection rules. Integrals II are

collectively parameterized with a quantity labelled ${}^{P}t_{\lambda}$, where $\lambda = \sigma, \pi_x, \pi_y$ according to the local symmetry speciation of the '*d*' functions being considered. Actually the operators *er* comprise three—*ex*, *ey*, and *ez*—for light polarized in different directions and '*d*' and '*d*'' may then have the same *or* different symmetry labels. It can be shown,[22] non-trivially, that separate parameters for *ex*, *ey* and *ez* and for '*d*' ≠ '*d*'' are not required, however. Integrals III similarly lead to parameters labelled ${}^{F}t_{\lambda}$. Integrals IV have been shown[22] to yield very little intensity in molecules with either bipyramidal or antibipyramidal geometries (to which very many chromophore structures actually approximate); we do not discuss them further here. Note that we parameterize local electric-dipole moments in this model with ${}^{P}t_{\lambda}$ and ${}^{F}t_{\lambda}$ which thus have the dimensions of electric-dipole moments, while the e_{λ} described in the preceding section are energies. There is a parallel between the CLF energy and transition parameters so far as their subscripts are concerned but an important difference with respect to the ${}^{L}t_{\lambda}$ ($L = P,F$) superscripts. This "double layer" of parameterization in which ${}^{P}t_{\lambda}$ relate to *d-p* mixing and ${}^{F}t_{\lambda}$ relate to *d-f* mixing provides a new and useful probe of the electron distribution in the M-L bonds, as we now discuss.

I have emphasized that our intensity model addresses relative intensities only. It follows that the absolute magnitudes of the various *t* parameters are without significance while their relative magnitudes are of the essence. Insofar that the amounts of metal *d*–metal *p* and metal *d*–metal *f* may be significant, empirical ${}^{P}t_{\lambda}/{}^{F}t_{\lambda}$ ratios obtained by fitting to experimental spectra may provide some information, but that will be overlain with factors arising from parity mixing *via* the M-L interactions. However, direct metal-metal parity mixing will usually be the minor contributor, and then it is possible to make some qualitative predictions. In these circumstances, the coefficients *c* of (1) are common for *p* and *f* character mixing, and the *P:F* ratios (meaning ${}^{P}t_{\lambda}/{}^{F}t_{\lambda}$) are determined by two-center expansions like (2). As noted earlier, the expansion coefficients *a* in (2) depend upon bond length and upon the radial forms of the ligand functions being expanded. Qualitative arguments have been presented,[27] and supported by idealized numerical computations[27] using Sharma's expansion relationships that lead to useful, general predictions about *P:F* ratios. They are that ${}^{P}t_{\lambda}/{}^{F}t_{\lambda}$ in any given ligation are expected to be larger for shorter bond lengths and/or fatter (greater lateral extension) bonds.

The doubling of the parameter set for the intensity model relative to the energy model might have been expected to render optimization procedures more difficult; in practice, few such problems have been

encountered, intensity analysis often converging more "cleanly" than energy ones. The gain from the doubling, however, is the further commentary upon bonding electron distribution afforded by these *P:F* ratios. For example, intensity contributions associated with metal-chlorine bonds are typically dominated by *d-f* parity mixing as evidenced by low ${}^{P}t_{\sigma}/{}^{F}t_{\sigma}$ ratios in these long bonds with relatively poor donor ligands; by contrast, high ${}^{P}t_{\sigma}/{}^{F}t_{\sigma}$ ratios and a predominance of *d-p* mixing are usual for metal-amine ligations involving shorter bonds and stronger donors.

As for the CLF model for energies, the completion of the intensity model involves the superposition of contributions from local ligations and the evaluation of all relevant matrix elements within the full many-electron basis of the appropriate metal d^n configuration. This is all described elsewhere.[22] Both energy and intensity models are general in that they are applicable on the same footing regardless of central metal, ligand set or chromophore geometry. While this last is true, much more needs to be said about centrosymmetric systems. Before doing so, however, it is worth emphasizing that the *er* operators are vector operators, relating to different polarizations. All calculations automatically involve the computation of intensity distributions for the incident light electric-dipole oriented quite generally with respect to the chromophore structure. This means that both magnitudes and polarization directions are computed from the common set of parameters. Appropriate spatial averages are formed when comparison with solution absorption spectra is desired. Otherwise the model provides a ready account of the polarized spectra to be obtained from single-crystal spectroscopy. One example[28] of the quality of agreement afforded by our model is shown in Fig. 3.

A particular consequence of the vectorial nature of the light electric-dipole operator is that, in centrosymmetric chromophores, an electronic displacement induced by light in one bond is matched by an equal but diametrically opposed displacement in the centrically related bond. In short, for the chromophore as a whole, the superposition of local electric-dipole moments yields a null result and we recover the well-known rule that '*d-d*' transitions are inactive in centric systems. The model described so far—a so-called "static" model—is therefore useful only for acentric chromophores. As very many interesting chromophores are centric, this constitutes a severe limitation upon the approach. The "static" model[22] addresses parity mixing that is permanently present. I now describe a recent extension[29,30] to the model—a "vibronic" model—that relates to parity mixing which is induced during *ungerade* molecular vibrations.

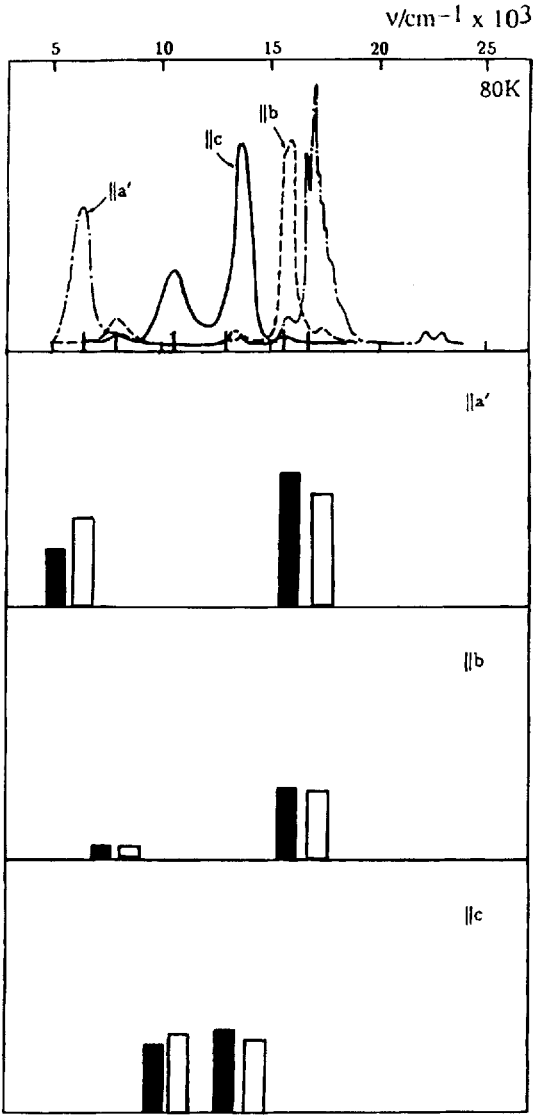

FIGURE 3 The single-crystal, polarized spectra of $CoCl_2(PPh_3)_2$. Solid and open bar graphs refer to observed and calculated band areas, respectively. Although calculated intensities are scaled overall for best reproduction of observed intensities, a common scale has been applied to all three polarizations.

The complex vibrations which molecules undergo may be decomposed into combinations of simultaneous, uncorrelated "normal modes" of nuclear motion. In centrosymmetric chromophores, some normal modes retain a center of symmetry—even or *gerade* modes—while others do not—odd or *ungerade* vibrations. The nuclear motions are very slow compared with the displacements of electron density that occur during the electronic transitions with which we are concerned. Light incident upon a macroscopic sample of material effectively "sees" molecules "frozen" in all possible nuclear configurations that occur within their various vibration cycles. Those molecules encountered in *acentric* configurations within *ungerade* modes suffer a degree of odd-parity mixing into their *d* functions. The '*d-d*' transitions may then be partly allowed as for acentric static molecules. Overall, the resulting intensities are expected, and found, to be weaker than in the corresponding acentric chromophores because the average degree of such parity mixing is less in molecules vibrating about a centric, "non-mixing", equilibrium structure than in permanently acentric species. Generally, one expects that the magnitude of parity mixing in vibrating centric systems to be related to the magnitude of nuclear displacements from their centric equilibrium positions; experimentally, the intensities of bands for centric chromophores do decrease with decreasing temperature. Equally generally, nuclear displacements are greater for low-frequency vibrations than for high-frequency ones. Bending vibrations are usually "softer"—of lower frequency—than stretches. For this reason, as well as for considerations of theoretical and parametric tractability discussed elsewhere,[29,30] our vibronic CLF model therefore focusses upon just *ungerade bending* modes. Several successful analyses[30–33] along these lines lend confidence to this starting point.

Because complex nuclear motions involve *uncorrelated* normal modes, the total intensity arising in any system is just the sum of intensities arising from each mode separately. Our modelling may therefore be illustrated quite generally by consideration of just one mode; in particular, of one *ungerade* bend. Recall that, in the basic "static" model, locally induced electric dipoles are parameterized by the ${}^{L}t_{\lambda}$: in centric chromophores the senses of these induced dipoles for diametrically opposite ligations are opposed so that contributions to intensity cancel. Within the small displacements of harmonic bends, changes in bond character are expected to be negligibly small so that the same *magnitudes* of the ${}^{L}t_{\lambda}$ parameters obtain throughout the vibration. The *directions* of the locally induced dipoles, however, do change. It is possible to refer these changes

in dipole orientation to the equilibrium nuclear frame and to parameterize them with "dynamic" ${}^{L}t_{\lambda}(D)$ parameters. Two important results have emerged[29]: (a) these dynamic contributions cancel for oppositely sited pairs of ligands undergoing *gerade* vibrations (as is, of course, required), and (b) for *ungerade* bends, the "dynamic" parameters are simply the ${}^{L}t_{\lambda}$ for the "static" model multiplied by the root-mean-square angular displacements undergone by the vibrating ligands. Note that these angular displacements are vectorial in the sense that the directions of ligand tangential motion are as important as their magnitudes. Altogether, therefore, our vibronic modelling is structured analogously to the "static" one and employs the same parameter set. It can be implemented once we know what ligand displacements occur in the various normal bending modes.

That information is available from normal coordinate analysis of the appropriate vibrational spectra. The NCA is performed by standard methods[34,35] which, of course, are completely independent of the electronic spectra we seek to interpret. All required RMS angular displacements are determined concurrently with the optimization of the vibrational force field to observed vibrational frequencies. Two further advantages flow from our vibronic approach. One concerns the temperature dependences of vibronically allowed '*d-d*' transitions in that these depend upon the temperature dependencies of the RMS ligand displacements—which may be estimated from the NCA procedures—rather than upon changes in bond character (presumed negligible) and hence in the ${}^{L}t_{\lambda}$ parameter values. Experience to date supports this. The second gain relates to those chromophores whose geometry deviates a little from centric. In such cases, intensity may arise from *both* static and dynamic sources. Our model handles this complication automatically and with no increase in the degree of parameterization. The ${}^{L}t_{\lambda}$ required for the static contribution serve also (after appropriate multiplication by RMS bending amplitudes for each normal mode) for the dynamic contributions.

A recent study[33] illustrates this point. Tris(ethylenediamine)nickel(II) ions strictly possess D_3 symmetry, suffering[36] a small "antiprismatic twist" with respect to the notionally ideal O_h precursor, as in Fig. 4. The CLF energy parameter set comprises just $e_{\sigma}(\mathrm{N})$ for these chemically equivalent amine ligations and provides an essentially unique fit to the '*d-d*' transition energies with $e_{\sigma}(\mathrm{N}) = 4010\ \mathrm{cm}^{-1}$. The lack of ligand π functionality of these ligands means that only ${}^{P}t_{\sigma}$ and ${}^{F}t_{\sigma}$ parameters are required for the intensity analysis. However, as only relative intensities

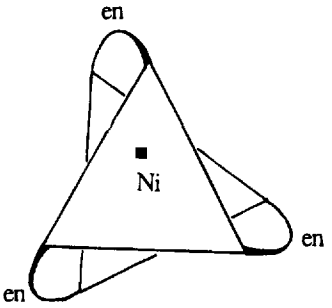

FIGURE 4 The D_3 symmetry of the $[Nien_3]^{2-}$ ion.

are being studied, the ratio ${}^{P}t_{\sigma}/{}^{F}t_{\sigma}$ remains as the only free variable. All appropriate RMS ligand displacements for ten bending modes were estimated beforehand by NCA using Wilson's GF matrix method[34] for some 34 vibration frequencies. An easy optimization of the one intensity variable yielded the agreement between calculated and observed band intensities shown in Table I. In passing, we note how the relatively high value (4) for ${}^{P}t_{\sigma}/{}^{F}t_{\sigma}$ fits well with earlier experience from the purely "static" model and other chromophores. Table II shows the relative contributions to intensity deriving from static and all vibronic sources.

A further test of the efficacy of the intensity model relates to the relative contributions to intensity from static and dynamic sources. Only static sources may contribute to the phenomenon of circular dichroism (CD), and Table I also shows how well the experimental CD in $[Ni(en)_3]^{2+}$ is reproduced—without further parameterization. The CD experiment records the differential absorption of left- and right-circularly polarized light. Theoretically, the sign and magnitude of the so-called "rotatory strength"—as determined by CD spectroscopy—is given by (the imaginary part of) the product of magnetic-dipole and electric-dipole matrix elements for a given transition.[37] We have calculated the electric-dipole moments within our intensity model already, and magnetic-dipole moments are computed in the same way that we have calculated paramagnetic moments for years (see, for example, Ref. 10). So, apart from some programming complexity, extension of the model for the analysis of CD is straightforward. Leaving aside the (admittedly central) conclusions of the analysis, the results of one other energy + (unpolarized) intensity + CD analysis[38] are summarized in Fig. 5, for the *pseudo*tetrahedral chromophore $CoCl_2$(α-isospartein) shown in Fig. 6.

TABLE I

Comparison of observed and calculated intensities for $[Ni(en)_3]^{2-}$

	Intensity Distribution					
	σ		π		axial CD	
band/cm^{-1}	obs.	calc.	obs.	calc.	obs.	calc.
9000–15000	24.2	23.0	30.1	30.6	−957	−952
15000–24000	18.6	20.7	9.9	10.2	−36	−42
28000–32000	17.3	15.5	a	7.9	−7	−6

[a]Transition obscured by charge-transfer feature.

TABLE II

Relative contributions from static and vibronic sources to the linearly polarized spectra of $[Ni(en)_3]^{2+}$

	Intensity Contribution			
	σ		π	
band/cm^{-1}	static	vibronic	static	vibronic
9000–15000	4.9	18.1	19.4	11.2
15000–24000	12.2	8.5	0.1	10.1
28000–32000	9.1	6.4	0.0	7.9

Altogether then, the intensity models sketched here share a similar generality with the CLF model for transition energies, applicable to any metal, ligand set, or complex geometry on an equal footing. To date, the models have again been exploited analytically in order to explore the electron distribution in bonds by reproduction of observed spectra. However, that process has generated increasing experience with the magnitudes of the various $^{L}t_{\lambda}$ parameters that are required, an experience upon which the present spectral-prediction facility will draw.

BANDWIDTHS

The comparisons between calculated and observed intensity distributions presented in Figs. 3 and 5 represent integrated band intensities as bar graphs. Attempts to reproduce real spectra have, of course, to include estimates of band profiles. In principle, these are as difficult to calculate as total molecular energies or absolute intensities so that we are obliged to consider approximate models in practice. We have adopted the simplest

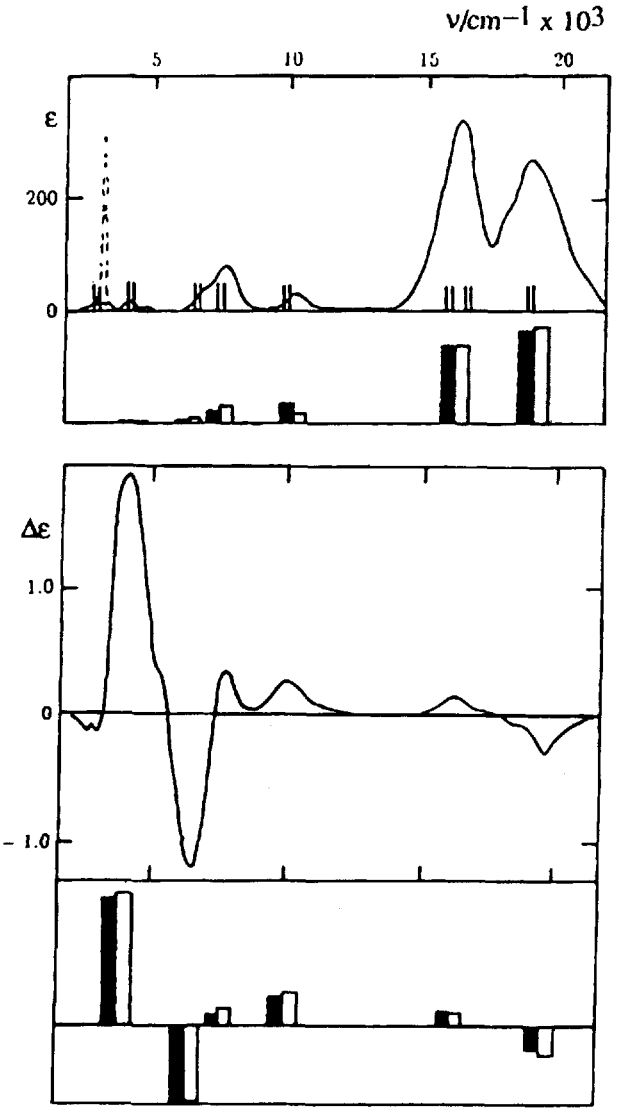

FIGURE 5 Extinction coefficients, ε, for $CoCl_2$ spartein (top) and differential extinction coefficients, $\Delta\varepsilon = \varepsilon_L - \varepsilon_R$ (bottom). Calculated transition energies are shown with the experimental unpolarized spectrum. Solid and open bar graphs show comparison of observed and calculated intensities. No further scaling is involved when reproducing the CD spectrum. Broken lines also indicate a non-'*d-d*' transition at ca. 3000 cm^{-1}.

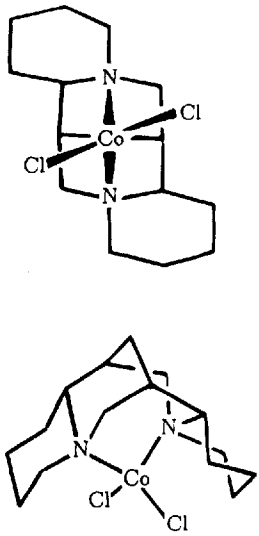

FIGURE 6 The chiral distortion in $CoCl_2$ spartein arises from Cl · · · spartein crowding.

of schemes. We presume the band profiles in wavenumber space to be gaussian in shape and their relative widths to be governed by the slopes of their transition energies with respect to small changes in all energy parameters. The thinking behind the latter assumption is as follows.

Progressions of the enabling vibration (if required, as in vibronic cases) are not seen but those of any totally symmetric vibration are—though they may not be well, or even at all, resolved. The width of a '*d-d*' absorption band is largely determined by the variation in the ligand-field parameters with changing geometry. This will be most acute for changes in bond length; a "textbook" example is that Δ_{oct} is predicted by various models to vary approximately with the inverse fifth power of bond length. We might therefore expect bandwidths to be determined predominantly by the magnitude of a symmetrical "breathing mode." We make the assuredly crude estimate that relative bandwidths are proportional to the relative changes in transition energies following a 5% change in all e_λ parameter values. No doubt this recipe could be improved upon, and it is certain that the procedure is less soundly based than our calculation of intensities (band areas).

The computation of a complete spectral trace for '*d-d*' transitions then requires one further variable; namely, the constant of proportionality just

referred to—in effect, a "mean bandwidth" for the whole spectrum. Figure 7 illustrates the level of success enjoyed[31] by this approach for a planar $[CuCl_4]^{2-}$ chromophore.

THE SPECTRAL-PREDICTION FACILITY

Our prediction of complete spectral traces for '*d-d*' transitions involves two main building blocks: a "look-up" table and/or predictive algorithms for the parameters relating to transition energies, intensity distributions and mean bandwidths; and a fast computational facility to implement the models summarized in the last three sections. Work on the former has barely begun but the latter is complete. In outline, the complete package may take the following form.

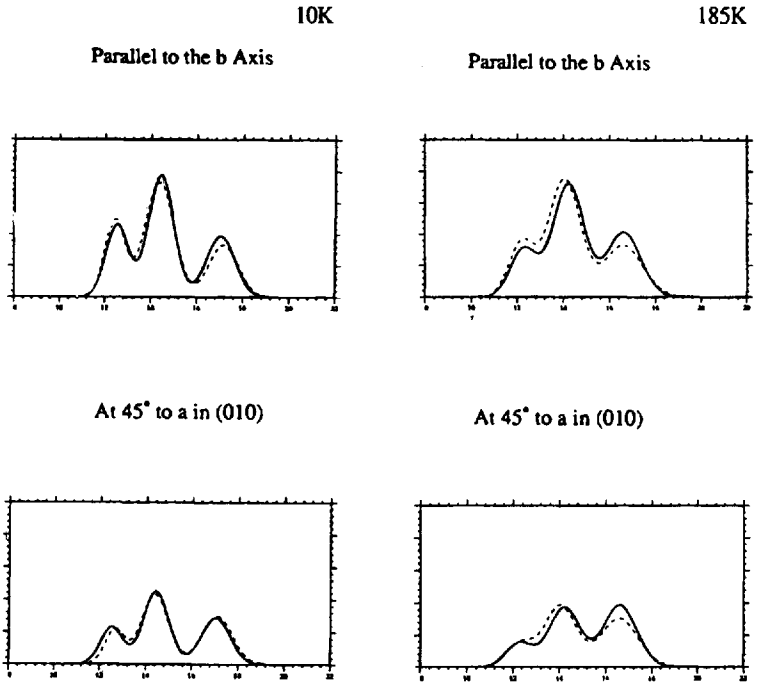

FIGURE 7 Observed (—) and calculated · · · spectral traces at 10 and 185 K for bis(*N*-methylphenylethylammonium)tetrachlorocopper(II) for two polarisations. The chromophore is the planar $[CuCl_4]^{2-}$ moiety.

Step 1. Using interactive graphical presentations with a workstation or PC, the user describes the coordination geometry and metal oxidation state to be examined. In the present "mock-up" condition, a list of coordinates is presented. In future, we shall graft on an ability to manipulate bonds using a mouse or window buttons. In the longer term still, the inclusion of a geometry optimizer (perhaps using molecular mechanics or other methods) would be an exciting goal.

Step 2. Currently, the presentation of energy parameters (B and C for interelectron repulsion, ζ for spin-orbit coupling, and CLF e_λ variables for the ligand-field potential) and of intensity parameters (the CLF ${}^{L}t_\lambda$ variables together with normal bending mode, ligand displacements for centric or near-centric chromophores) is made directly by the user. We are currently working on the construction of "look-up" tables for these various quantities and on the design of algorithms for their interpolation and extrapolation as required. This is a non-trivial task, and part of its implementation requires further work to test the sensitivity of predicted spectra to parameter values estimated in this way. Our plans include a facility to upgrade the parameter-guessing package easily with the advent of more data from independent analytical studies. Even in final form, the user would have the option of overriding any automatically generated parameter values.

Step 3. The calculations are performed. At the moment, they are restricted to unpolarized spectra, for it is most likely that experimental data on a new compound relate to solution spectra only. Extension to circular dichroism will not be difficult. For the unpolarized spectra, four stages of computation are involved but they run consecutively without recourse to the user. In (i), transition energies and associated (angular) wavefunctions are computed using the energy parameters provided; a second calculation using parameter values multiplied by 1.05 is also performed for stage (iii) below. In stage (ii), relative intensities—band areas—are computed using the wavefunctions and energies from (i) together with the ${}^{L}t_\lambda$ parameters and any necessary details of molecular vibrations. In stage (iii), relative bandwidths are estimated from the differential energies computed in (i), gaussian profiles for each transition are calculated using the relative band areas of (ii) together with the relative bandwidths and a multiplicative mean bandwidth factor, and then summed to yield the complete spectral trace. The three stages (i) to (iii) are schematically indicated in Fig. 8. Stage (iv) involves the output of this trace onto the computer screen and as hardcopy, if desired. One further refinement, however, has been included at this point. The area under the computed trace is filled with the color that

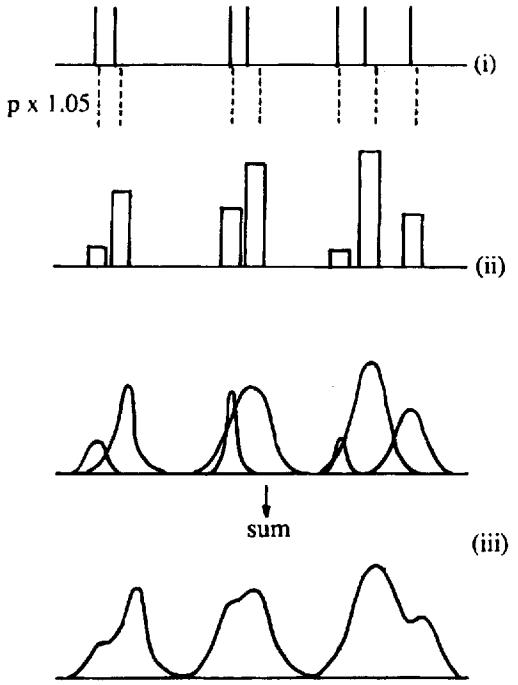

FIGURE 8 The stages of simulating a '*d-d*' spectral trace. In (i) transition energies and wavefunctions are computed. Transition energies are also calculated using parameter values increased by 5% to estimate relative bandwidths. In (ii) relative spectral intensities are calculated. In (iii), gaussians are assigned to each transition according to (ii), the relative bandwidths and the overall mean bandwidth scale factor, and then summed.

such an absorption spectrum would generate. The computation takes into account the responses of the normal human eye together with the varying amplitude of the computed trace. The full-color figures at the end of the present article (see Color Plates I and II) reproduce some examples of the whole procedure (subject, of course, to any limitations in the color printing process). By way of example, the whole of step 3 takes about five seconds for a d^7 chromophore on a Sun IPC Workstation. In due course, we shall implement the facility on PCs too.

Step 4. This is by way of "tinkering". It is possible to replot the trace and color, using a different mean bandwidth; that takes about one second only. It is also possible to add a changing baseline to the plot to simulate the effects of high-lying charge-transfer bands as detailed below.

I finish with a brief commentary upon the calculated spectra presented in the color plates. The plots, numbered 1 to 12, present absorbances on a relative scale; apart from some weakening automatically generated in 3 for a completely spin-forbidden spectrum, all hues are of full saturation in recognition of our inability to calculate *absolute* intensities.

1. The spin-allowed transitions and pink color of octahedral hexaaquocobalt(II) ions.
2. The same for hexaaquonickel(II) ions but with inclusion of spin-forbidden transitions, only one of which is visible—within the "doublet" at ca. 14000 cm^{-1} by stealing intensity from its closest spin-allowed neighbor.
3. The spin-forbidden spectrum of the d^5 hexaaquomanganese(II) ion. Note the sharpness of some "spin-flip" transitions.
4. Jahn–Teller splitting in the d^9 hexaaquocopper(II) ion is unresolved within the single broad band envelope (nominally $^2E_g \rightarrow {}^2T_{2g}$ transition.)
5. The color of verdigris and of similarly coordinated "octahedral" copper(II) ions arises from the addition of some violet absorbance due to the tail of high-lying charge transfer bands. These are not calculated by our procedures so that their energy and intensity are merely simulated by a very intense band at a user-selected frequency. While no claim for veracity is therefore made for "corrections" of this kind, they usefully illustrate the effect of charge-transfer bands upon hue.
6. The royal blue color of $[CoCl_4]^{2-}$ ions. Both spin-allowed and spin-forbidden transitions are included. The change from "mid-blue" to the observed "royal blue" arises from the weak, spin-forbidden bands at 16000 to 19000 cm^{-1}.
7. The $[CuCl_4]^{2-}$ ions in Cs_2CuCl_4 possess flattened tetrahedral geometry. The calculated (and observed) '*d-d*' transitions all occur in the near infrared region and the program computes no *visible* hue. For reasons of presentation, a pale grey shade is assigned by the program to such "colorless" chromophores.
8. The true color of Cs_2CuCl_4 crystals is a golden yellow. This plot shows how that originates in the tail of a charge-transfer band encroaching into the visible.
9. Similar encroachments in Cs_2CuBr_4 fall to lower energy due to the greater softness of bromine relative to chlorine, and the brick-red color results.

10. Tetrahedral $[NiCl_4]^{2-}$ ions are blue, though many students are unaware of the fact!
11. Many "tetrahedral" nickel(II) complexes involve distorted geometries arising, for example and as here, from ligation to Schiff bases of various kinds. These compounds are usually "leaf green" in color. "Leaf green" is not a true spectral color, and the occurrence of the only absorbance in the visible at the "green" part of the spectrum (at its inverse, of course, for absorbance) yields instead only a "traffic-light" green as shown here. Adjustments of bandwidth or frequency are unable to produce the required "leaf" green.
12. These Schiff-base complexes invariably possess low-lying charge-transfer transitions. The encroachment of one such into the visible adds a yellow component to the spectrum in 11 and yields the desired hue.

I have chosen these examples for their teaching potential and in order to cover a reasonably broad range of application. Complexes with geometries possessing little or no symmetry are equally accessible so that all the topics suggested at the beginning of this article may be addressed. Some readers may be disappointed that so many of the examples include contributions from charge-transfer tails. Even though we are unable to model these effects properly, they do have considerable educational value. In any case, their inclusion or not affects perceived hues rather than the '*d-d*' spectral trace itself which has, of course, been modelled in full.

Overall, the approach is only approximate, and it undoubtedly trades on happy chances that prediction of broad-band spectra offers. Provided fine detail is not sought from this technique, we should have a useful and constructive facility.

Acknowledgments

I am most grateful to Dr. A. J. Bridgeman for his judgement and critical comments.

References

1. C. K. Jørgensen, R. Pappolardo and H.-H. Schmidtke, J. Chem. Phys. **39**, 1422 (1963).
2. C. E. Schäffer and C. K. Jørgensen, Molec. Phys. **9**, 401 (1965).
3. C. E. Schäffer, Struct. Bonding **5**, 68 (1968) and references therein.

4. C. E. Schäffer, Struct. Bonding **14**, 69 (1973) and references therein.
5. M. Gerloch, in *Understanding Molecular Properties*, eds. J. S. Avery, J.-P. Dahl and A. Hansen (Reidel, 1987), p. 111.
6. A. J. Bridgeman and M. Gerloch, Prog. Inorg. Chem., in press.
7. M. Gerloch, J. H. Harding and R. G. Woolley, Struct. Bonding **46**, 1 (1981).
8. M. Gerloch and R. G. Woolley, Prog. Inorg. Chem. **31**, 371 (1984).
9. R. G. Woolley, Molec. Phys. **42**, 703 (1981).
10. M. Gerloch, *Magnetism and Ligand-Field Analysis* (Cambridge University Press, Cambridge, 1983).
11. B. R. Judd, Phys. Rev. **127**, 750 (1962).
12. G. S. Ofelt, J. Chem. Phys. **37**, 511 (1962).
13. S. F. Mason, R. D. Peacock and B. Stewart, Molec. Phys. **30**, 1829 (1975).
14. B. R. Judd, J. Chem. Phys. **70**, 4830 (1979).
15. F. S. Richardson, J. D. Saxe, S. A. Davis and T. R. Faulkener, Molec. Phys. **42**, 1401 (1981).
16. E. M. Stephens, S. Davis, M. F. Reid and F. S. Richardson, Inorg. Chem. **23**, 4607 (1984).
17. M. F. Reid and F. S. Richardson, J. Chem. Phys. **79**, 5735 (1984).
18. M. F. Reid and F. S. Richardson, J. Phys. Chem. **88**, 3579 (1984).
19. M. T. Devlin, E. M. Stephens, F. S. Richardson, F. S. Van Cott and S. A. Davis, Inorg. Chem. **26**, 1204 (1987).
20. D. E. Henrie, R. L. Fellows and G. R. Choppin, Coord. Chem. Rev. **18**, 199 (1976).
21. Y. M. Poon and D. J. Newman, J. Chem. Phys. **17**, 4319 (1984).
22. C. A. Brown, M. Gerloch and R. F. McMeeking, Molec. Phys. **64**, 771 (1988).
23. M. Gerloch, Coord. Chem. Rev. **99**, 199 (1990).
24. M. Gerloch and E. C. Constable, *Transition Metal Chemistry* (VCH, Weinheim, 1994).
25. R. R. Sharma, Phys. Rev. A **13**, 517 (1976).
26. C. J. Ballhausen and A. D. Liehr, J. Molec. Spect. **2**, 342 (1958).
27. C. A. Brown, M. J. Duer, M. Gerloch and R. F. McMeeking, Molec. Phys. **64**, 825 (1988).
28. C. A. Brown, M. Gerloch and R. F. McMeeking, Molec. Phys. **64**, 771 (1988).
29. M. J. Duer, S. J. Essex, M. Gerloch and K. M. Jupp, Molec. Phys. **79**, 1147 (1993).
30. A. J. Bridgeman, S. J. Essex and M. Gerloch, Inorg. Chem. **33**, 5411 (1994).
31. M. J. Duer, S. J. Essex and M. Gerloch, Molec. Phys. **79**, 1167 (1993).
32. A. J. Bridgeman and M. Gerloch, Molec. Phys. **79**, 1195 (1993).
33. A. J. Bridgeman, K. M. Jupp and M. Gerloch, Inorg. Chem. **33**, 5424 (1994).
34. E. B. Wilson Jr., J. C. Decius and J. C. Cross, *Molecular Vibrations* (McGraw-Hill, New York, 1955).
35. S. Califano, *Vibrational States* (Wiley-Interscience, New York, 1976).
36. J. D. Korp, I. Bernal, R. A. Palmer and J. C. Robinson, Acta Cryst. **36B**, 560 (1980).
37. L. Rosenfeltd, Z. Physik **52**, 161 (1928).
38. N. D. Fenton and M. Gerloch, Inorg. Chem. **29**, 3718 (1990).